

Modelling coastal low-level wind-jets: does horizontal resolution matter?

Raza Ranjha^{1,2} · Michael Tjernström^{1,2}  · Gunilla Svensson^{1,2}  · Alvaro Semedo^{3,4} 

Received: 27 December 2014 / Accepted: 12 October 2015 / Published online: 12 November 2015
© Springer-Verlag Wien 2015

Abstract Atmospheric flows in coastal regions are impacted by land–sea temperature contrasts, complex terrain, shape of the coastline, among many things. Along the west coast of central North America, winds in the boundary layer are mainly from north or northwest, roughly parallel to the coastline. Frequently, the coastal low-level wind field is characterized by a sharp wind maximum along the coast in the lowest kilometre. This feature, commonly referred to as a coastal low-level jet (CLLJ), has significant impact on the climatology of the coastal region and affects many human activities in the littoral zone. Hence, a good understanding and forecasting of CLLJs are vital. This study evaluates the issue of proper mesoscale numerical model resolution to describe the physics of a CLLJ, and its impact on the upper ocean. The COAMPS[®] model is used for a summer event to determine the realism of the model results compared to observations, from an area of supercritical flow adjustment between Pt. Sur and Pt. Conception, California. Simulations at different model horizontal resolutions, from 54 to 2 km are performed. While the model produces realistic results with increasing details at

higher resolution, the results do not fully converge even at a resolution of only few kilometres and an objective analysis of model errors do not show an increased skill with increasing resolution. Based on all available information, a compromise resolution appears to be at least 6 km. New methods may have to be developed to evaluate models at very high resolution.

1 Introduction

In meteorology the term “low-level jet” is used to describe a broad number of wind phenomena caused by different processes and observed over nearly all parts of the world (Bonner 1968; Uccellini and Johnson 1979; Li and Chen 1998), all featuring a wind-speed maximum near the surface. Thermal processes related to differential land–sea heating are vital to one class of jets: the coastal low-level jet (CLLJ), the topic of this paper. Such jets are found along many coastal regions (Zemba and Friehe 1987; Doyle and Warner 1991; Douglas 1995; Burk and Thompson 1996; Holt 1996; Nicholson 2010; Rahnja et al. 2015; see Ranjha et al. 2013 for a global climatology). At locations with significant along-coast topography, the terrain can have profound effects on the flow, with local-scale enhancements of the wind. Several previous studies have investigated the influence of local coastal terrain on the CLLJ (Winant et al. 1988; Samelson 1992; Burk and Thompson 1996; Ström et al. 2001), in particular on how points and capes along the coast lead to substantial accelerations and decelerations of the flow (Beardsley et al. 1987; Tjernström and Grisogono 2000).

CLLJs appear predominantly along subtropical west coasts (Winant et al. 1988). Ranjha et al. (2013) presented

Responsible Editor: J.-F. Miao.

✉ Michael Tjernström
michaelt@misu.su.se

¹ Department of Meteorology, Stockholm University, 10691 Stockholm, Sweden

² Bolin Center for Climate Research, Stockholm University, 10691 Stockholm, Sweden

³ Escola Naval-CINAV, Lisbon Naval Base, Alfeite, 2810-001 Lisbon, Portugal

⁴ Instituto Dom Luiz, Faculdade de Ciências, University of Lisbon, Campo Grande Edifício C1, 1749-016 Lisbon, Portugal

a global climatology of CLLJs and found a combination of characteristics that promotes persistent CLLJs: a significant land–sea temperature contrast, hence persistent CLLJs are mainly a summertime phenomenon, and beneficial large-scale wind climatology, setting up an along-coast background wind field. The interplay between background wind direction and the coastline orientation is critical. Hence, along some coastlines, for example the US West Coast, there is a significant annual cycle with persistent CLLJs only in summer in response to the migration of the North Pacific high-pressure region and the resulting wind direction along different parts of the California coast. In contrast, CLLJs exist around the year along the South America coast, with a long straight north–south-oriented sub-tropic coastline, but moves north and south due to the seasonal migration of the South Pacific high pressure. CLLJs have a significant impact on the atmospheric forcing of the coastal ocean, driving large sea surface temperature (SST) reductions due to upwelling forced by Ekman transport and pumping, enhanced in the lee of coastal points (e.g. Marchesiello et al. 2003).

The coastal environment is demanding for numerical weather prediction (NWP) models, with a mixture of large- and small-scale complex processes, i.e. strong baroclinicity with sharp gradients in temperature and pressure, large contrasts in surface roughness, and sometimes also steep topography. Many studies have indicated that regional climate modelling, allowing higher horizontal resolution, capture more regional detail than general circulation models in climate scenarios (Giorgi et al. 1994; Jones et al. 1995; Chen and Fu 2000; Ju and Wang 2006; Gao et al. 2008; Salathé et al. 2008), and that increased resolution allows for a better description of finer scale structures of synoptic and mesoscale weather systems defining the climate of a region (e.g. Leung et al. 1996; Machenhauer et al. 1998; Christensen and Kuhry 2000). A model's horizontal resolution is of course also very important for the simulation of the surface climate, strongly influenced by fine-scale forcing such as from topography and land use distribution (Giorgi and Mearns 1991). However, while it is commonly assumed that increasing horizontal resolution provides better surface forcing, offering a better representation of topographic and other land surface features, and that sub-grid scale physical processes are also better represented, scale interaction is complicated and increasing the resolution is not necessary a general solution to all modelling problems.

The dependence of model skill in predicting regional-scale features on the model resolution has long been a key issue in the numerical weather prediction (NWP) community. Forecast model experiments have indicated that small-scale error growth is rapid and hence that forecast skill in general is ultimately determined by skill on the synoptic

scales. Higher resolution should improve the representation of the synoptic scales which then feeds back on larger scale. For mesoscale circulations determined by fine-scale topography or other sharp surface features, it is expected that higher resolution does improve the result by providing a better representation of the surface forcing. CLLJs belong to this class of mesoscale motions. Several studies indicate that the effective dynamic resolution might be 5–10 times poorer than the numerical resolution (Bengtsson et al. 2012; Skamarock 2004). Imposing forcing at a scale 5–10 times smaller than that a model is actually capable to resolve dynamically is in itself not unproblematic. While it is recognized that coarse-resolution models cannot reproduce many important small-scale features, the question of optimal resolution arises: Is there a threshold resolution beyond which further refinement of the model resolution brings no significant improvement and will this threshold depend on location and physical processes?

Many studies have considered this aspect (e.g. Mass et al. 2002; Colby 2004) but with different outcomes, partly depending on the phenomena studied. Hence, the primary objective of this study is to explore the significance of the horizontal resolution in the context of the CLLJ characteristics. An underlying assumption is that there exists a dynamic scale of the flow that should determine the optimal resolution, and that results from increasingly higher resolutions should converge in structure although not necessarily in detail. Beyond this hypothetical optimal resolution, the basic structure of the simulated CLLJ should, therefore, remain unchanged while details may be added. This dynamic scale for the CLLJ problem is assumed to be on the order of the mountain Rossby radius of deformation (Overland and Bond 1996; Bond et al. 1996) determining the seaward reach of coastal influence, for the present case assumed to extend ~ 100 km from the coast (Rogers et al. 1998). Hence, results from simulations with a model with a poorer resolution than $O(10$ km), as is the case for most climate models, are expected to be inferior since they will not resolve dynamics at this scale.

For the CLLJ climatology in Ranjha et al. (2013), the ERA-Interim reanalysis (Dee et al. 2011) was used, at about 70 km resolution. The climatology revealed several areas where CLLJs are prevalent, many of which have not received much scientific interest although some of them are known for their oceanic upwelling characteristics. Also, Rahnja et al. (2015) showed that in ERA-Interim data some aspects of the Oman CLLJ are difficult to distinguish from the so-called Somali (or Findlater) jet. However, ERA-Interim is a data assimilation product and some spatial structures may have been resolved because of the impact of observations. Most published simulations for the California CLLJ have been performed at resolutions in the ~ 10 km range (e.g. Rogers et al. 1998; Hsu et al. 2007; Dorman and

Koraćin 2008), although some detailed studies have been performed at resolutions down to <1 km (e.g. Burk and Haack 2000). Simulations of CLLJs along the South-American coast were conducted at even coarser resolution (Tonizzo et al. 2011) but also here dedicated studies have been carried out at higher resolution (3 km, Rahn et al. 2011). The CLLJ off the coast of Portugal was simulated at ~9 km resolution by Soares et al. (2014) while the Oman jet was simulated at 6 km by Rahnja et al. (2015).

For the purpose of this study we will consider the CLLJ as a mesoscale phenomenon and explore the effects on its bulk structure by different resolutions, including effects by major headlands, capes and bays. By smaller or fine-scale details we consider the effects of details within these coastal structures. We use a mesoscale model, the US Navy's COAMPS® model, to simulate a real case at different resolutions with the aim to investigate the impact of varying resolutions on a CLLJ, using results from a nested simulation. This implies only one simulation, simultaneously at several resolutions. The paper is organized with a brief discussion on US West Coast CLLJs in Sect. 2, while the model and the observations are described in Sect. 3. This is followed by a brief evaluation in Sect. 4 while the main results are found in Sect. 5. Section 6 includes a brief discussion of the effect of different resolution on some objective scores, and some concluding comments are found in Sect. 7.

2 US West Coast coastal jets

The summertime CLLJ off the coast of California, USA, has been a target of several studies (Samelson 1992; Burk and Thompson 1996; Rogers et al. 1998; Dorman et al. 1999; Burk et al. 1999; Tjernström 1999; Tjernström and Grisogono 2000; Ström et al. 2001; Haack et al. 2005; Rahn and Parish 2007). Neiburger et al. (1961) provided a summary of the climatology of the California CLLJ. During summer the mean sea-level pressure field and winds off this coast are under the influence of the location of the North Pacific high at about 40°N and a thermal low over the southwest deserts of USA. The large-scale flow is predominantly northerly to north-westerly, with coast-parallel winds along the California coast (e.g. Ranjha et al. 2013). Due to the persistent and strong low-level baroclinicity between the cool ocean and the heated continent, the maximum pressure gradient is found at the coast, decreasing landward and seaward. The subsidence associated with the offshore high pressure helps set up an elevated inversion that is sloping downward to the coast. Through the thermal wind relation, the sloping inversion generates an increasing northerly flow with decreasing altitude across the inversion, until it is balanced by turbulent friction (Burk and Thompson 1996). The low-level

wind profile thus attains a distinct wind-speed maximum just below the marine inversion base at the location where the inversion slope is the largest, typically at heights around 100–500 m. The CLLJ hence requires a persistent favourable background flow (Ranjha et al. 2013) and a strong land-to-sea temperature contrast, in a configuration where heated land is “to the left (right)” in the flow direction on the northern (southern) hemisphere.

Field measurement (e.g. Zemba and Friehe 1987; Beardsley et al. 1987; Rogers et al. 1998) quote wind speeds in excess of 30 m s^{-1} in the core of a CLLJ. The CLLJ also goes through a diurnal cycle with minimum winds at night and morning and maximum winds in the late afternoon or early evening. This is a lagged effect from the diurnal land–sea temperature contrast (Beardsley et al. 1987; Tjernström and Grisogono 2000; Dorman and Koraćin 2008): maximum inland solar heating occurs at local noon and the maximum temperature somewhat later while the inertia in the geostrophic adjustment process lags the wind response into the late afternoon or evening.

Along much of the US West Coast, the coastal terrain reaches higher than the near-shore marine atmospheric boundary layer (MABL), thereby confining the CLLJ between the terrain, the capping inversion and the surface. In this setting, the flow becomes sensitive to effects by changes in the “coastal sidewall”; points, capes and bays, e.g. Cape Mendocino, Pt. Reyes, Pt. Sur and Pt. Conception (e.g. Fig. 1 in Dorman and Koraćin (2008)). This type of flow was analysed by Winant et al. (1988) using a non-rotational and inviscid shallow-water channel-flow analogue. The strong and coastward sloping MABL inversion sets the stage in two ways: by generating high wind speeds in the CLLJ and by providing a good approximation of a shallow-water system. Hence, Winant et al. (1988) categorized the flow using the shallow-water definition of the Froude number: $Fr = U (g'h)^{-1/2}$. Here, U is the flow speed, h is the MABL depth and g' is the reduced gravity

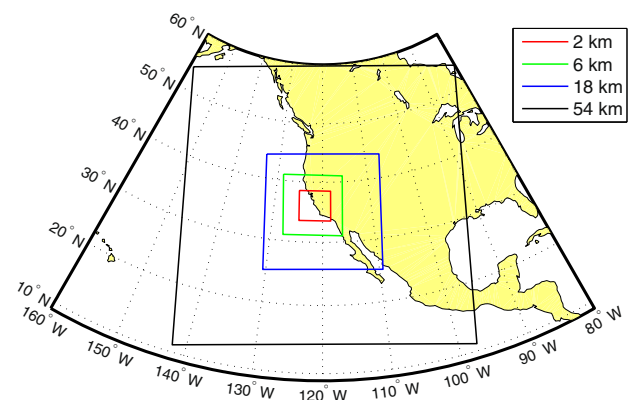


Fig. 1 COAMPS® model domains used in the study, from outermost to innermost domain with horizontal resolution of 54, 18, 6, and 2 km, respectively

defined as $g' = g \Delta T T^{-1}$ where g is the gravity, T is the temperature and ΔT is its jump across the MABL-capping inversion. In this context, Fr compares the flow speed to the group (or phase) speed of shallow-water waves, $(g'h)^{1/2}$; these long waves are responsible for the geostrophic adjustment of mass and wind fields (e.g. Dorman and Koraćin 2008); in the shallow-water context group and phase speed are the same.

As the coastline turns “away” from the flow at a point or cape, the downwind “channel” widens. Continuity causes the near-coast MABL to thin, the inversion slope increases and the flow accelerates. If the upstream Fr is close to unity, shallow-water waves cannot propagate upstream, against the flow, prohibiting an upstream geostrophic adjustment to the local pressure perturbation. Winant et al. (1988) refer to this as trans- or supercritical flow. Waves can, however, propagate across the flow and hence the influence of a cape or point expands offshore with downstream distance, forming a fan-like pattern (e.g. Winant et al. 1988; Ström and Tjernström 2004); hence the term “expansion-fan” dynamics. This explains local wind speed maxima observed downwind of capes and points along the US West Coast (Burk et al. 2001). Conversely, as the flow decelerates for example by surface friction, or if the coastline turns into the flow again, implying a “narrowing” channel, there will be a point along an air-parcel trajectory where the wind speed exactly equals the shallow-water wave group/phase speed: $Fr \equiv 1$. Shallow-water waves generated downwind of this point propagate upwind but stagnate at this point, amplify and break. This is usually referred to as a “hydraulic jump”.

In a continuously stratified real MABL, affected by non-linearity, turbulence and the Earth rotation, flow patterns become more curved and smooth; confined to the near-coast MABL roughly within a mountain Rossby radius of deformation, $L_R = Nh/f$. Here N , the Brunt Vaisalla (or buoyancy) frequency, is used as a measure for the stability in the MABL-capping inversion, while f is the Coriolis parameter. The flow within this distance is often semi-geostrophic, as in a frontal zone (e.g. Cui et al. 1998). Still, the simple super/subcritical shallow-water theory describes the flow surprisingly well. For example, when observed CLLJ wind speeds at different distances from the coast and different distances downstream from a major headland are scaled using theoretical expansion-fan widths, the result collapses nicely (e.g. Ström and Tjernström 2004).

3 Model setup and observational data

We use the Coupled Ocean/Atmosphere Mesoscale Prediction System (COAMPS[®]) atmospheric model, developed at the US Naval Research Laboratory in Monterey,

California (see Hodur 1997 for an overview). COAMPS[®] is the US Navy’s operational regional forecast model, but has also been used in many scientific studies. It has been used widely in studies of marine weather off the US west coast, in particular for coastal jets (Thompson et al. 1997; Burk and Haack 2000; Haack et al. 2001; Wetzel et al. 2001), but has also been used for other studies in other regions (e.g. Tjernström et al. 2005; Steeneveld et al. 2008).

COAMPS[®] is a compressible non-hydrostatic model with the option of using nested domains, achieving affordable high resolution in areas of particular interest. Nesting involves embedding a higher resolution model domain in the outer parent domain. COAMPS[®] allows for subsequent domains nested inside each other, with a resolution increase by a factor of three for each new nest. We used one-way nesting, where each domain relies on its parent domain for lateral boundary conditions, but is otherwise independent. COAMPS[®] uses an Arakawa-C horizontal grid with a staggered terrain following σ_z vertical coordinate system. Vertical resolution is always a compromise, especially when running very high horizontal resolution. In the present study, the model was configured with 51 vertical levels and a model top at 10 hPa; the lowest model level is at 30 m with seven levels below 1 km and the MABL was typically resolved by 4–5 grid points in the vertical.

The nesting consisted of four domains (three nests) with a parent domain at 54-km and nests at 18, 6, and 2-km horizontal resolutions, respectively (Fig. 1). The outer model domain was forced at the lateral boundaries by the European Centre for Medium-Range Weather Forecasts (ECMWF) ERA-interim reanalysis (Dee et al. 2011) at 6-h resolution. SST was also taken from the ERA-interim to be consistent with the lateral boundary forcing, and was set constant in time for the simulation period. No observations were assimilated into COAMPS[®] during the continuous integration. Hence, this is a dynamic downscaling of a reanalysis and not a forecast experiment.

Physical parameterization schemes included long- and shortwave radiation (Harshvardhan et al. 1987), explicit moist physics (Rutledge and Hobbs 1983), cumulus convection (Kain and Fritsch 1990), and a “Level-2.5” higher order turbulence closure (Mellor and Yamada 1982). A simple surface energy balance scheme was used to compute the land surface temperature. To avoid problems with parameterized convection at higher resolution, the convection scheme was switched off for the two innermost nests (6 and 2 km).

The purpose of this study is to explore the behaviour of simulated CLLJs under different horizontal resolution. Hence we are interested in a physically realistic simulation to be able to explore the effects of the different resolutions

and, therefore, we base this study loosely on a real event from the summer of 2004. The model was integrated from 0000 UTC on 3 August to 2400 UTC on 10 August, conforming to a portion of the Naval Postgraduate School (NPS; Monterey, California) 2004 summer cruise on the R/V Point Sur (Semedo 2004), from which we have some offshore observations, in particular vertical soundings. Offshore vertical profiles are not available from operational observing systems. During this period the central coast of California was under the influence of the North Pacific High, cantered about 40°N over the ocean north of Hawaii, and the southwest US inland thermal low over the Mojave Desert. This synoptic pattern forced a roughly coast-parallel flow in the lower atmosphere between Cape Mendocino and Point Conception, favouring the development of a CLLJ. R/V Pt. Sur followed a track along the California Cooperative Oceanic Fisheries Investigations: lines 67, 70, 77 and 85 (CALCOFI; <http://www.calcofi.org/>). A brief evaluation allows us to check the realism of the model, using two types of observations. The NPS cruise provided a total of 26 radio soundings, numbered from 1 to 26; Fig. 2 shows the location for the first 24. We also use hourly 8-min averaged wind speed and air temperature observations from the National Data Buoy Center (NDBC; <http://www.ndbc.noaa.gov>) buoy 46028, located at 35.741°N , 121.884°W . On this buoy wind was measured at 5 m and temperature at 4 m above the surface.

4 Model assessment

Although this is not a model evaluation study, an analysis of the impact of model resolution on the CLLJ would be pointless if the model was unable to accurately simulate this type of flow. This ability has been demonstrated in

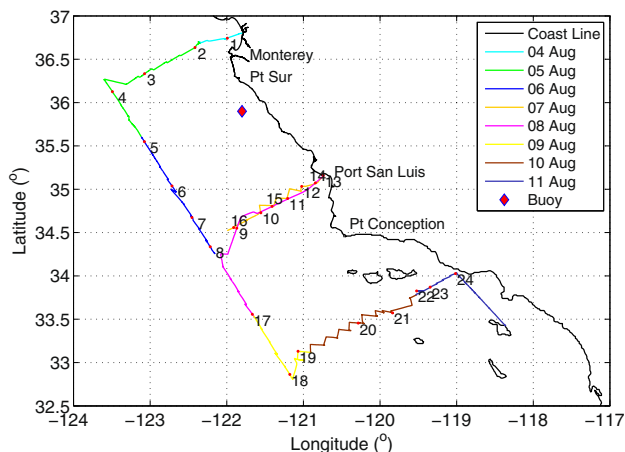


Fig. 2 NPS summer cruise 2004 by R/V Pt. Sur, showing the cruise track (coloured lines) and the radiosonde positions (numbers). The diamond represents the location of the NDBC buoy

several previous studies; in this section we only perform a brief model assessment, comparing model results to radiosonde observations and buoy data. It should be kept in mind that for this study, the initial atmospheric state as well as all large-scale forcing, including SST and lateral boundary conditions, come from ERA-Interim and that no observations were assimilated into COAMPS[®]. The priority here is not to optimize model performance as compared to observations; just to ascertain that the results are physically reasonable. Note that some of the figures discussed in this section also include the results from the different resolutions to avoid unnecessary repetition of plots; these results will be discussed in detail in the next section.

Figure 3 shows the wind vectors with colour shading for scalar wind speed at 30 m, for the 2, 6, 18 and 54-km resolution domains, respectively. The example is from 0500 UTC on 5 August 2004 and is typical for the structure near the CLLJ maximum. The model results display a wind speed maximum from Pt. Sur to Pt. Conception, roughly parallel to the coast; this is typical to what would be expected for a CLLJ. This wind-speed maximum appears to be part of an expansion fan/hydraulic-jump feature well known to exist in this region during strong north-westerly wind conditions (e.g. Winant et al. 1988; Samelson 1992; Tjernström and Grisogono 2000).

Figure 4 shows contours of Fr calculated at all marine grid points. The shallow-water Fr is here calculated from the MABL depth, temperature jump across the inversion, and the mean wind speed inside the MABL. Using the mean MABL wind speed as a shallow-water analogue is somewhat arbitrary and hence the exact demarcation of where the flow is supercritical or not should not be interpreted literally. Still, the flow is trans- or supercritical (at all resolutions) in a shallow band along the coast downstream of Pt. Reyes to the north of San Francisco Bay. This zone widens in a smoothly curved fan-like pattern south of Monterey Bay and Pt. Sur that reaches a width of about 150–200 km at the southern end of the domain. Inside this zone Fr consistently reaches supercritical values in a narrow band along the coast between Pt. Sur and Pt. Conception.

The corresponding east–west vertical cross section in Fig. 5 corroborates that the wind-speed maximum in Fig. 3 is part of a CLLJ. Note that these cross sections are taken at the latitude of the strongest CLLJ for each resolution, indicated by red lines in Fig. 3. The presence of the jet is clear, with a core in all nests with wind speeds up to 20 m s^{-1} . This again illustrates the capability of the model to capture the general characteristics of a CLLJ. Scanning through the simulation results with output every hour (not shown), the CLLJ structure is similar, although of course not exactly the same, each day.

Fig. 3 Surface wind fields at 30-m height showing the wind speed (m s^{-1} ; colour shading) and wind direction (arrows) for **a** 2-km, **b** 6-km, **c** 18-km and **d** 54-km resolution, on 5 August, 2004 at 0500 UTC. *Red lines* areas of vertical cross sections discussed in Fig. 5 and *black lines* the along- and across the shock like features of the jet in Fig. 11

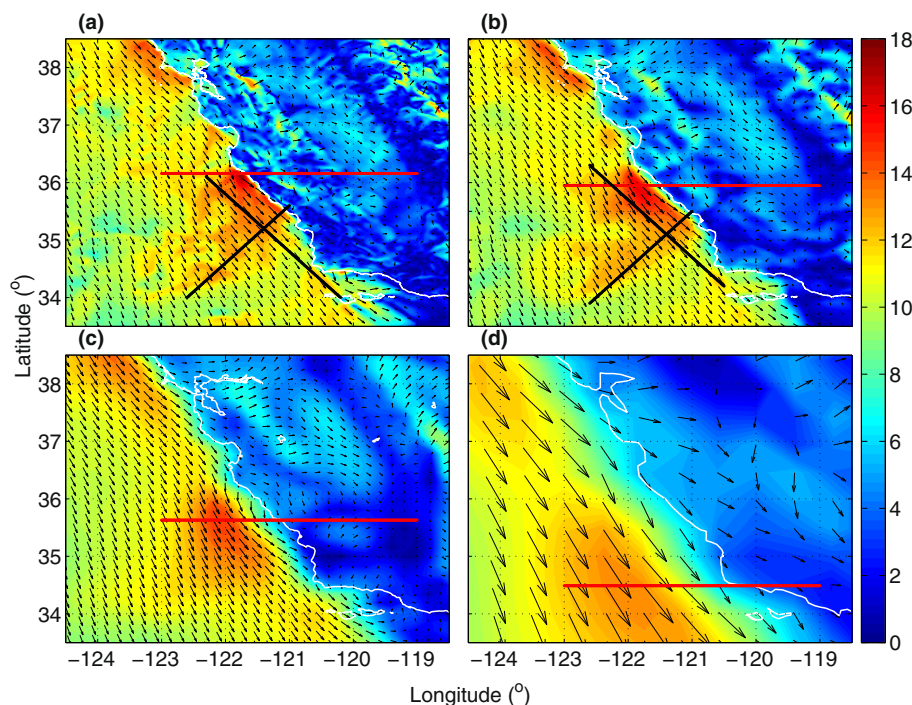
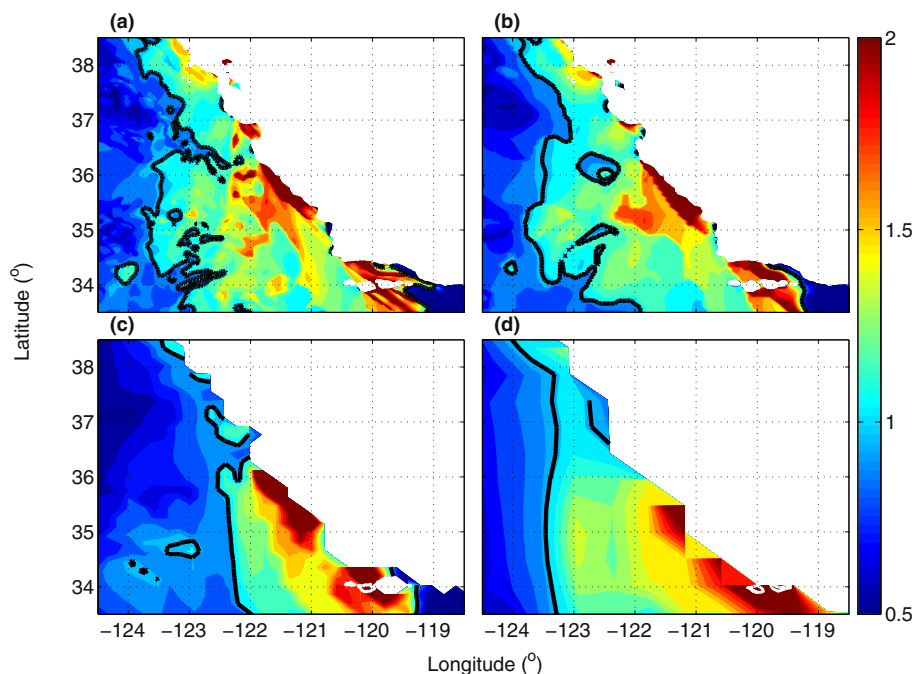


Fig. 4 Shallow-water Froude number (Fr) calculated from the model results for all marine grid points at **a** 2-km, **b** 6-km, **c** 18-km and **d** 54-km resolution, on 5 August, 2004 at 0500 UTC, corresponding to the wind fields in Fig. 3. Note that the coast line is outlined at the different model resolution



Figures 6 and 7 show examples of vertical profiles of potential temperature and wind speed, respectively, comparing model results with radio sounding observations for sounding locations 3 and 5 in Fig. 2. A shallow well-mixed MABL, capped by an inversion (Fig. 6) and the jet-like shape in the wind speed profile (Fig. 7) appears in both model results and observations. There are differences in

detail, in particular the model's wind speed is slightly on the low side especially at the core of the jet and slightly above, but the structure is well captured.

Figure 8 shows a more comprehensive evaluation, using data from all the available radio soundings. Here the model wind speeds and temperatures from the 2-km resolution domain were interpolated in time and 3D space to the 26

Fig. 5 Latitudinal vertical cross section of wind speed (m s^{-1} ; colour shading) and potential temperature (K; white solid lines) for **a** 2-km, **b** 6-km, **c** 18-km and **d** 54-km resolution, on 5 August 2004 at 0500 UTC. Note that the latitude is different in different panels; locations are selected at **a** 36.20°N , **b** 35.95°N , **c** 35.63°N , and **d** 34.50°N , according to the north–south location of the strongest coastal jet (see Fig. 3)

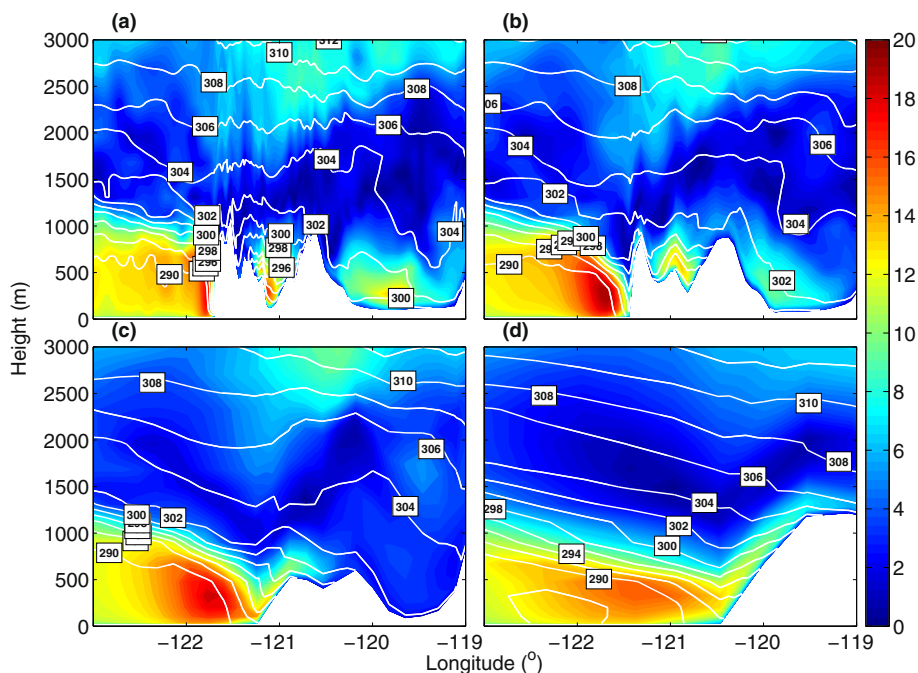
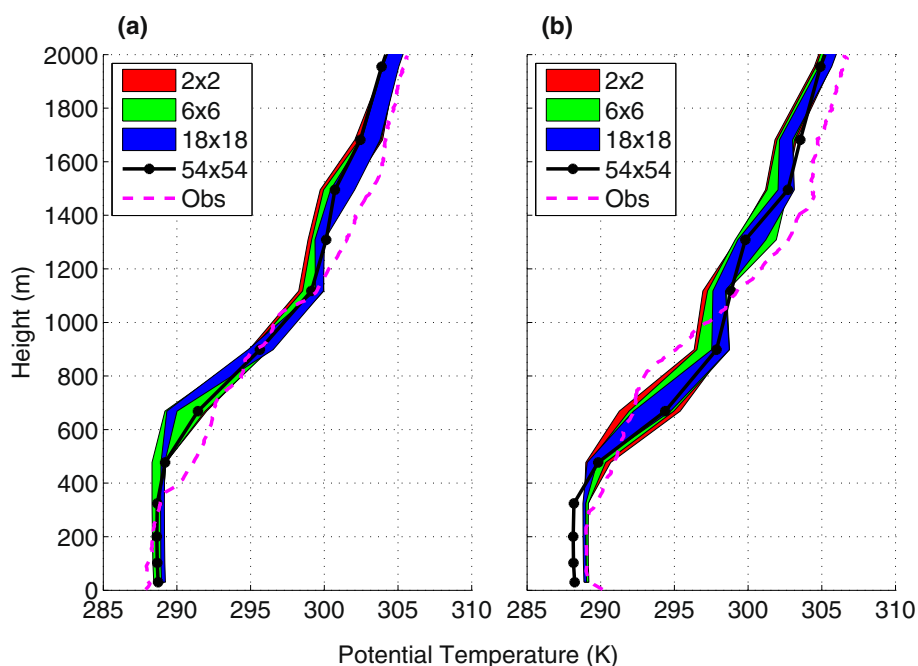


Fig. 6 Vertical profiles of potential temperature (K), from radio soundings and model simulations at different resolution on **a** 5 August, 2004, at 1000 UTC, and **b** 6 August, 2004, at 0100 UTC; these soundings were taken at locations 3 and 5, respectively, in Fig. 2. The higher resolution runs are portrait using the results in a 54×54 -km box around the nearest model profile; see the figure legend and the text for more details



soundings; however, the launch time for each sounding was used for each entire sounding and horizontal sonde drift was not accounted for. In general, the model is a few degrees colder on average throughout the whole troposphere (best fit line in Fig. 8a; also see Fig. 7); note that in general, higher potential temperature is from higher altitude. It is difficult to envision a modelled physical process that would cause such a bias over the ocean, constant for the entire height range. For example, an SST error would

likely affect the low-level temperatures more than those aloft, whereas temperature errors arising from problems in the model parameterizations would likely be a function of either altitude or temperature itself. This leads us to suggest that this systematic bias is likely inherited from ERA-Interim, initially and imposed at the lateral boundaries. A larger scatter for temperature, around ~ 290 to 300 K, is likely due to slight inconsistencies in inversion heights. A linear regression for wind speed indicates a relative wind-

Fig. 7 Same as Fig. 6, but for scalar wind speed (m s^{-1})

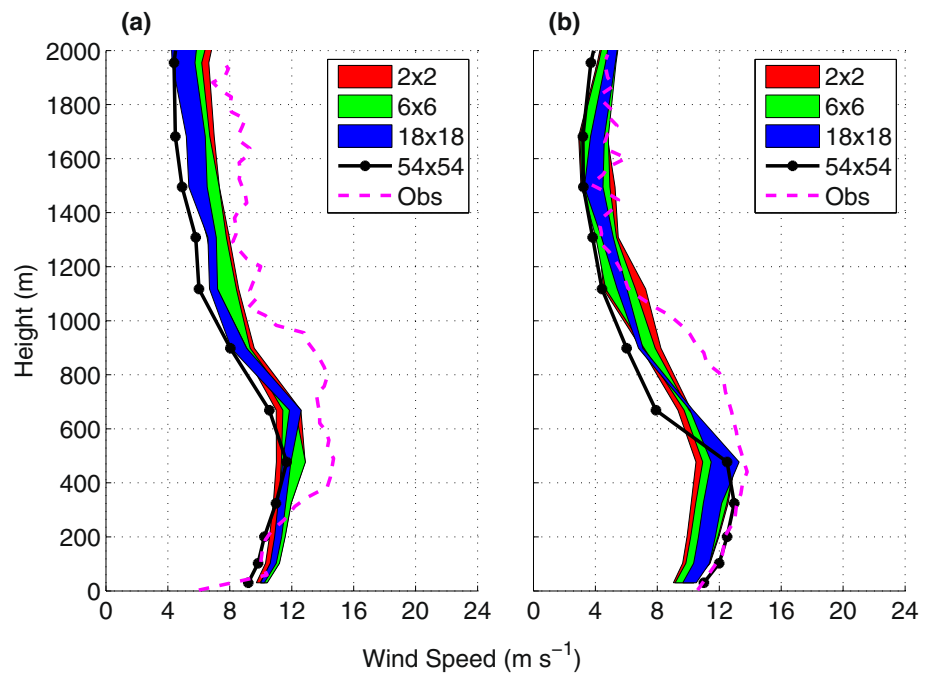
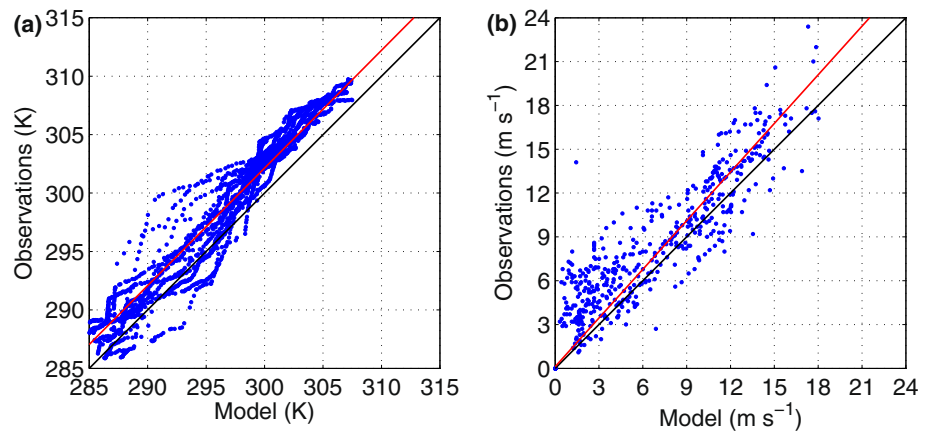


Fig. 8 Scatter plot of **a** potential temperature (K) and **b** wind speed (m s^{-1}), showing observations from all the soundings available (see Fig. 2) on the y-axis and the corresponding 2-km resolution model results on the x-axis, interpolated to observation locations. *Red line* trend line



speed error of $\sim -10\%$; modelled winds are increasingly too low with increasing wind speed. Additionally, there is a tendency for somewhat larger scatter and bias for the lowest wind speeds. Note that although near-surface winds are in general low, lower winds also appear aloft, above the CLLJ (see Fig. 7).

In Fig. 9, model results are compared with buoy observations, taken near the coast south of Pt. Sur (Fig. 2). Winds are interpolated from the lowest model level (at 30 m) to buoy observations at about 4 m (temperature) and 5 m (wind speed) above the surface using similarity theory. Figure 9a reveals a puzzling bias between the modelled air temperature and the observations; the model results are about $2\text{ }^{\circ}\text{C}$ warmer, regardless of resolution. At the same time the low-level temperature compared to the soundings (Figs. 6, 8a) is not nearly this much in error, in fact if

anything they indicate a slight cold bias. It is difficult to reconcile the relatively good agreement in MABL temperature in the soundings with such a large warm bias near the surface when comparing to the buoy data. One reason may be that the near-surface air temperatures close to the coast are in fact this low; for example, as a consequence of local upwelling not captured by the low-resolution ERA-Interim SST fields. This is supported by the fact that the SST used in the model is about $4\text{ }^{\circ}\text{C}$ warmer than the observed air temperature. It is, however, beyond the scope of this paper to determine if the apparent error is due to an observation error or unresolved SST gradients. The observed weak cooling trend in the air temperature over these 4 days is, however, picked up by the model, as well as the warming late on 8 August. There is no diurnal cycle in temperature, neither in the observation nor in the model.

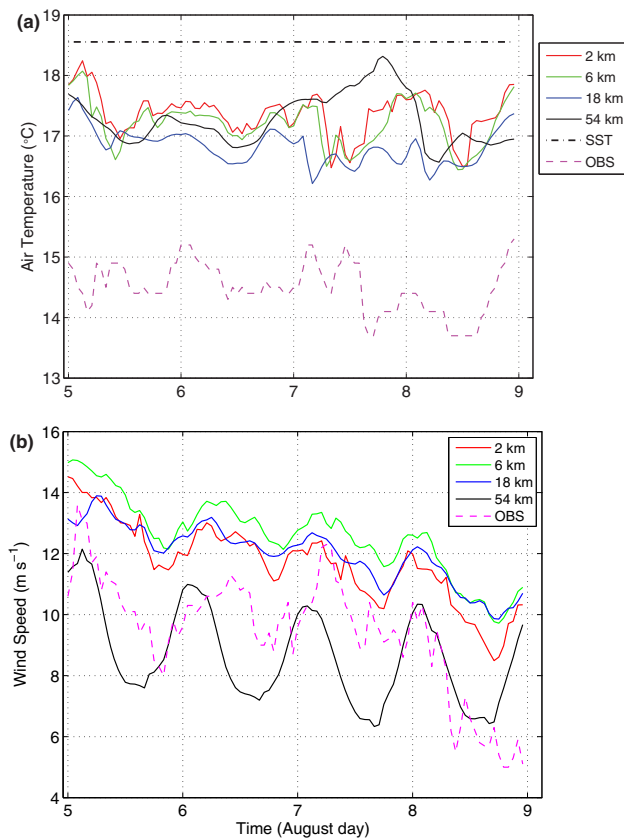


Fig. 9 Time series of near-surface **a** air temperature in $^{\circ}\text{C}$ and **b** scalar wind speed in m s^{-1} , the model at different resolutions (2, 6, 18 and 54 km; see legends) and from buoy 46028, for 5–8 August, 2004. Also shown in **a** is the (time constant) SST used in the model

Since these are from a near-surface marine location, where the temperatures will be strongly influenced by the SST, a diurnal cycle is not expected.

Simulated wind speeds (Fig. 9b) for all three higher resolutions are on top of each other and also in very good agreement with the observations, except for towards the end of the time series. Both the downward trend and the diurnal cycle are well captured, except that the diurnal cycle tends to be stronger in the observations. At the coarsest resolution, however, the wind speed is too low while the diurnal cycle is out of phase, appearing too early in the day. Except for the coarsest resolution, which is clearly inferior, it is difficult to determine what resolution provides the best result. Since this is a single point comparison, the exact position of the CLLJ is important, hence the poor results for the coarsest resolution is expected since its wind-speed maximum occurs far off shore (see Fig. 3). One may speculate in how the wind speed can be so close to the observations temperature while the temperature has such a large bias. This is in line with Tjernström (1999), where simulations with and without an observed SST reduction downstream of Cape Mendocino had only

marginal effects on the wind. This indicates that while the surface forcing from the atmosphere on the ocean is strong, the feedback from the reduced SST, and the corresponding increase in boundary layer static stability, only have minor effects on the CLLJ.

In summary, the model displays a CLLJ in line with expectations but also has some biases, which are different when comparing to soundings or buoy data. The soundings indicate the model is somewhat cold on average while the buoys indicate a warm bias near the surface. Similarly the soundings indicate slightly too low winds while the buoy comparison is fair, except for at the lowest resolution. Unfortunately, the buoy location, chosen because of its proximity to the modelled wind speed maximum and being on a reasonably uncomplicated stretch of the coast, neither inside a bay nor near a cape, makes a comparison between sounding and surface observations difficult. However, the temporal developments in the buoy observations are captured in the model. Recalling that the purpose of this paper is not a model evaluation, but the comparisons of model results on different resolutions, we conclude that the model behaves reasonably and features the main dynamic properties of the CLLJ.

5 The impact of horizontal resolution

Figures 3, 4 and 5 confirm that the model reproduces the expected larger and mesoscale features of summertime coastal flow in this region, it also illustrates substantial differences in the results as resolved by different nests, from coarser to finer horizontal resolution. A detailed comparison of the panels in Fig. 3, 4 and 5 reveals significant differences in location and structure of the jet and of the wind-speed maximum at the core of the jet. While the 54-km resolution results does show a broad region of higher wind speeds, with a maximum around 12 m s^{-1} , the core of the jet is quite far offshore and also displaced southward compared to the results from higher resolutions. Although the wind-speed maximum (Fig. 3d) and Fr (Fig. 4d) indicates expansion-fan dynamics, the features at the coarsest resolution have a very smooth and smeared-out character without sharp horizontal gradients. Given the typical Rossby radius of deformation ($\sim 100 \text{ km}$, e.g. Ström et al. 2001) the 54-km resolution is, as expected, not sufficient for a proper resolution of the impact of the coastline on the flow. In the 18-km resolution results, the wind-speed maximum is still located well offshore, while in the 6- and 2-km resolution results the highest wind speeds are found close to the coastline. The maximum near-surface wind speed increases from 12 m s^{-1} for the 54-km domain to 14 m s^{-1} for the 18-km, $16\text{--}17 \text{ m s}^{-1}$ for the 6-km and $17\text{--}18 \text{ m s}^{-1}$ for the 2-km resolutions,

respectively, as the core of the highest wind speeds moves closer to the coast with increasing resolution. Hence, it appears that 16-km resolution improves the results compared to 54-km, but that the large difference appears for the 6-km results. The 2-km results then add details to the 6-km results but do not change the main characters of the CLLJ.

Further inspection also reveals many smaller scale features present in the finer resolution, that fade away moving to coarser resolutions. While only weakly indicated at 54-km resolution, the 18-km resolution results separate the wind speed maximum into two (Fig. 3c), one northerly, north of San Francisco Bay, and one southerly, between Pt. Sur and Pt. Conception. This separation becomes even clearer in the 6- and 2-km domains. For example, at 2-km resolution (Fig. 3a) there are sharp low wind-speed bands ($<10 \text{ m s}^{-1}$) extending from the coast and seaward. One originates at the coast between the San Francisco and Monterey Bays and a weaker band also appears north of Pt. Sur, with wind speeds down to $\sim 8 \text{ m s}^{-1}$. Although not further discussed here, lee effects from the Catalina Islands are also only visible at the higher resolutions.

At 18-km resolution (Fig. 3c), signs of an along-flow wind-speed gradient approximately along 34.2°N starts to appear. In the 6-km resolution results (Fig. 3b), this develops into a feature with an appearance similar to that of a shock oriented perpendicular to the coast, somewhat north of Pt. Conception, possibly a hydraulic jump. This is a region where the coast turns slightly into the flow where such a feature could be expected. In the 2-km resolution (Fig. 3a), this feature remains at roughly the same location but also develops along-shock structures. These structures are also indicated in the Fr-fields (Fig. 4), but only for the two highest resolutions, see Fig. 4a, b. A proper description of a shock requires resolution even higher than 2 km. Burk and Haack (2000) simulated a shock at Pt. Sur using COAMPS[®] at a $1/3 \text{ km}$ resolution. However, the dynamics resulting in a hydraulic jump, the super-to-subcritical transition, does occur also at low resolution, while the jump itself will be poorly represented.

Clearly the 2-km resolution results show significant details that may, however, be difficult to evaluate from observations. On balance, the 6-km resolution results retain most of the mesoscale structure from the 2-km domain, but without some of the details. The southerly and northerly jet regions are clearly visible and well separated, and the flow perturbations at capes and points are clearly reproduced. These structures rapidly fade away while moving from the 6- to 18-km resolution. At 54-km resolutions, most of the mesoscale structure is smeared out and the CLLJ and its features are pushed far offshore.

Figure 5 shows east–west vertical cross sections of wind speed (colour shading) and isentropes (white lines) for the different resolutions. Note that the terrain is plotted at the

corresponding model resolution and that since the coastal topography is resolved differently at different resolution, these cross sections are taken at the maximum CLLJ wind and hence at different latitude. The CLLJ is seen for all model resolutions, consistent with the surface winds in Fig. 3. As the resolution becomes coarser, the CLLJ becomes weaker and broader, and also moves away from the coast, similar to what was seen in the horizontal near-surface wind fields. This is a result of changes in the MABL inversion slope (Tjernström and Grisogono 2000). For the 54-km resolution results, this slope is almost linearly downward from the western edge of the model domain to the coastline. All the three nested domains show a more realistic structure, with a lower inversion slope well offshore and a gradual transition to a more rapidly sloping inversion approaching the coastline. The enhanced near-coast slope acts to localize the CLLJ and higher resolutions have a steeper final slope to the coastline closer to the coast. The CLLJ is found right below the inversion with the maximum wind speed where the inversion slope increases. Consequently, the cross-flow width of the jet core is shrinking and the maximum wind speed is increasing with increasing resolution.

An example of added dynamical detail at the highest resolution is indicated in the potential temperature field. A closer examination of the 2-km resolution results (Fig. 5a) reveals a wave-like structure in the marine inversion. Browsing through several cross sections hour by hour (not shown) gives an impression that this feature actually propagates offshore and we speculate that this may be a shallow-water wave propagating away from the coast while being swept downstream, as is expected in this region. Other details in the 2-km resolution results are the inland features. This not being the focus of this study; we only mention briefly here the inland jets in the Salinas River Valley (around 121°W) and in the San Joaquin valley ($119^\circ\text{--}120^\circ\text{W}$), both of which are well-known features.

The effects of resolution on spatial location and intensity of the CLLJ are summarized in Fig. 10, showing wind-speed isotachs for every second m s^{-1} starting at 13 m s^{-1} . In Fig. 10b, the corresponding cross-coast patterns are presented, here with respect to the model coastline at each resolution; the coastline is located slightly differently in the different domains and the cross sections are at slightly different latitude (see Fig. 3). In the horizontal plane, the area with near-surface winds larger than 13 m s^{-1} is roughly the same in the 2- and 6-km results (Fig. 10a), while the results from both the 18- and 54-km results are substantially farther offshore. In the three higher resolutions, and with this definition, the width of the jet is $\sim 100 \text{ km}$, as expected from the discussion earlier on L_R earlier. In the coarsest resolution the CLLJ is very far offshore, displaced south and much too wide. In the

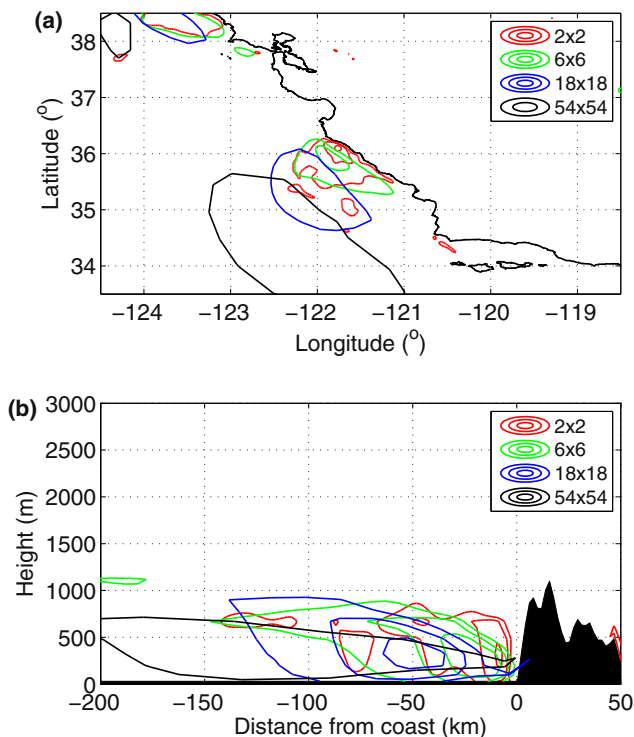


Fig. 10 Outlines of coastal jets in **a** the horizontal and **b** vertical plane illustrating the effect of resolution on the spatial location of jet for (see legend) 2-, 6-, 18- and 54-km resolutions. See Fig. 3 and the text for discussion

vertical, the region of the highest winds is again similar in both size and location for the two higher resolutions (Fig. 10b). However, the detailed structure of the CLLJ is different, so that the very highest wind speeds in the 2-km resolution are much narrower and closer to the coast, consistent with the differences in the shape of the coastward inversion slope discussed earlier (e.g. Fig. 5).

Figure 11 shows the CLLJ characteristics in cross sections along and across the shock-like feature (black lines in Fig. 3) north of Pt. Conception for the 2- and 6-km resolutions. Especially in the 2-km resolution results the expansion fan is indicated as a kink in the southward slope of the wind-speed maximum (Fig. 11a). This is well inside the $Fr \sim 1$ line in Fig. 4, but is consistent with the shape of the fan; note the ambiguity in the definition of the shallow-water Fr from a three-dimensional model as discussed earlier. There are also indications of a lower Fr roughly along the shock-like features (Fig. 4). The maximum wind speeds increase southward from Pt. Sur and then go through a rapid transition with decreasing wind speeds through the shock before entering a new expansion fan initiated at Pt. Conception. Interestingly the MABL, here defined as the well-mixed layer below the base of the inversion, does not seem to deepen across the shock as one would have expected from the shallow-water flow analogy.

Instead the thickness of the inversion layer increases, reducing the stability in the capping inversion. A similar height adjustment occurring in the capping inversion, rather than by changing the MABL depth, was also observed in airborne observations of so-called “coastally trapped wind reversals” (Nuss et al. 2000). Although proven a useful analogue for the coastal MABL in this region, the shallow-water concept does not include a realistic inversion; note that the continuously stratified form of Fr involves N . Across the CLLJ at this transition, the jet exhibits a dual structure (Fig. 11b, d) with two wind-speed maxima. While the structures are smoother in the 6-km results (Fig. 11d), the basic features are similar, again confirming the relative similarity between the 2- and 6-km resolution results.

Not only the wind stress itself but its curl is important for forcing of the upper coastal ocean. Large values of wind-stress curl has been observed in association with CLLJs and coastal headlands as the location of the maximum wind speeds separates from the coast downstream of a cape. This can sometimes be seen as low-SST areas in satellite imagery. The lowest SSTs in lee of coastal features are often well correlated with these features (e.g. Tjernström and Grisogono 2000; Pickett and Paduan 2003). Figure 12 shows the wind-stress curl for the 2-, 6-, 18- and 54-km resolutions, computed from the surface wind-stress fields corresponding to the near-surface winds in Fig. 3. Strong localized forcing of the coastal ocean is indicated in the 2- and 6-km resolution results. The strength and detail of this forcing is drastically reduced and redistributed at the 18- and 54-km resolutions, suggesting that 2-km, or possibly even higher, resolution may be required to properly resolve this forcing. This was not the case for the general features of CLLJ, hence the optimal resolution may be dependent on the feature of interest.

In summary, the impacts of resolution increase are complex and for some characteristics there seem to be an optimum resolution while in other cases not. For the gross structure of the CLLJ there seems to be a convergence of the results at the 6-km resolution, considering both the horizontal and vertical structure. The 6-km results also capture a fair portion of the detailed structures. The 2-km results, of course, even more so but the change going from 18- to 6-km resolution is significantly larger than going from 6- to 2-km resolution. An additional factor speaking for 6 km as a candidate for “optimal resolution” is that in the coarser resolutions the CLLJ is significantly displaced off the coast and also somewhat southward. However, using other ways to define the CLLJ, such as the detailed cross-coast shape of the wind maximum and the value of the very highest winds, these results do not seem to converge, even though 2 km is a much smaller scale than the theoretical offshore distance for effects by the coast,

Fig. 11 Wind speed cross sections (a, c), across- and (b, d) along the shock like feature in jet core (see *black lines* in Fig. 3), for 2- and 6-km resolutions, respectively

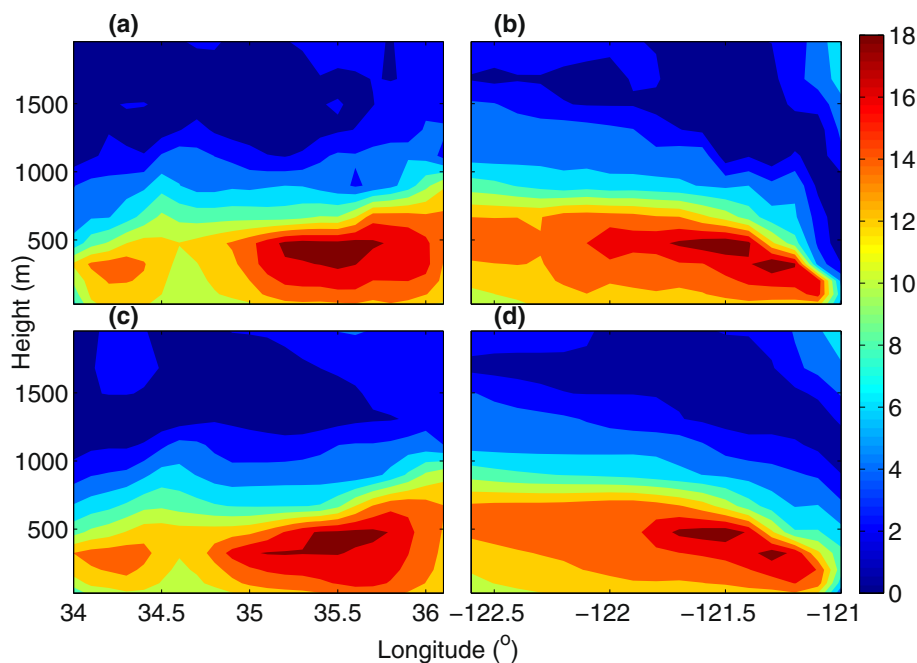
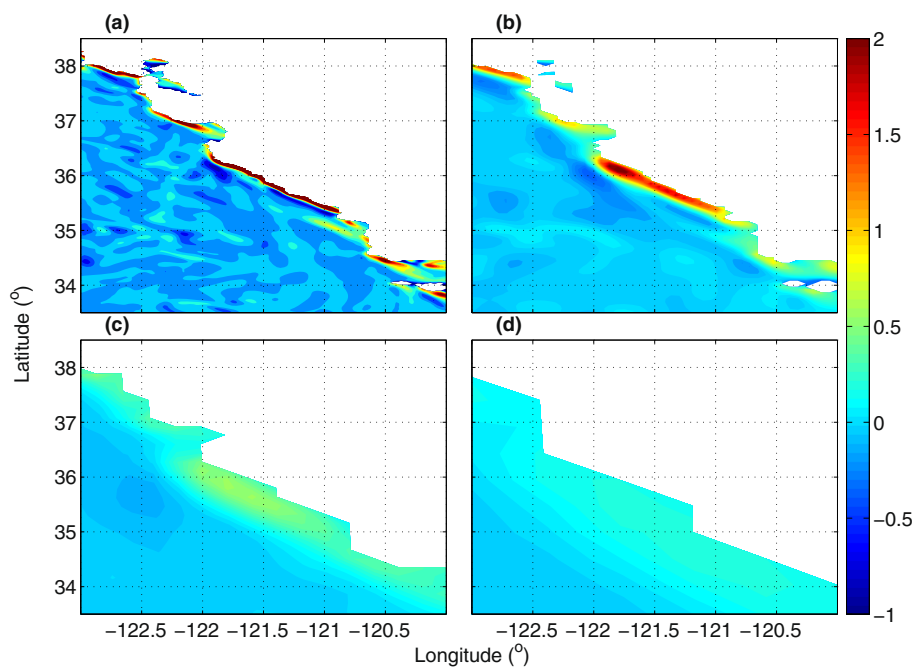


Fig. 12 Wind stress curl (N m^{-2}) at a 2 km, b 6 km, c 18 km and d 54 km on 5 August, 2004, at 0500 UTC



~ 100 km. Hence, for each threefold increase in resolution the finer scaled structure of the CLLJ keep changing, with higher wind speeds in a more localized maximum closer to the coast. In fact, the absolute maximum wind speed increases nearly linearly with resolution from 18- to 2-km resolution (not shown). For a more subtle parameter, such as the surface wind-stress curl, the changes with increasing resolution are larger both in terms of the extreme values and area. Still, it seems that the 6-km resolution captures

most of the jet features, while the coarser resolutions do not in several important aspects.

6 Model resolution and objective scores

In the previous section, we explored the convergence of the CLLJ structure as resolution increased without paying too much attention to if this convergence is correct, other than

that it appears plausible given what we know about CLLJs. While it is evident that an increase in the horizontal resolution provides more detail, and also changes some aspects of the structure of the CLLJ, the question arises if it can be objectively demonstrated that higher resolution agrees better with observations.

Some information to address this is encapsulated in Figs. 6 and 7. Instead of interpolating, we show model data from a 54 km² area for all domains. Hence, the coarsest resolution results are shown by a single line from the grid point nearest the observations while the higher resolution results are represented by shaded areas, spanning all the profiles from the neighbouring 27 × 27, 9 × 9 and 3 × 3 grid points in the model for the 2-, 6-, and 18-km domains, respectively. This additionally illustrates the horizontal variability within the 54-km resolution grid box for all resolutions higher than 54 km. Figure 6 shows the potential temperature profiles for two cases. The 2-km results has the largest spatial variability, while the variability decreases with decreasing resolution, as less grid points are available and the higher resolution details get averaged out. Somewhat surprisingly, the horizontal variability in the high-resolution results is smaller in the MABL than aloft. The results in the MABL are also closer to the soundings than aloft. The capping inversion is somewhat sharper in the high-resolution runs, although the vertical resolution is unchanged, while the coarse-resolution results seem to follow the extreme values in the higher resolution results rather than their median. This means that the 54-km results are not an average of the results from the higher resolutions.

Similarly, the modelled and observed mean wind speeds are shown in Fig. 7. Again the 2-km results have the largest variability and are the closest to observations. Going to coarser resolutions the 6-km profiles exhibit similar features as the 2-km profiles while the 54-km wind-speed profile seems to follow the minimum in the 2-km ensemble of profiles. Increased resolution thus adds variability, as expected, but the 54 × 54-km² average of the 2-km resolution results is again not the same as the 54-km resolution results. The mean of the 2-km resolution wind speeds over the larger domain are more often than not higher than the wind speed from the 54-km resolution results.

The time series of modelled and observed near-surface temperature and wind speed at the buoy location (Fig. 9) also show differences with varying resolution. For the temperature, the results from the 2- and 6-km domains are again quite similar, while the largest difference appears in the 54-km domain, especially during 7 August. The temperature bias, defined as model minus observations, ranges from 2.0 to 2.5 °C while correlations are low. The 18-km results has the smallest while the 54-km results has the largest errors; the difference between the resolutions is,

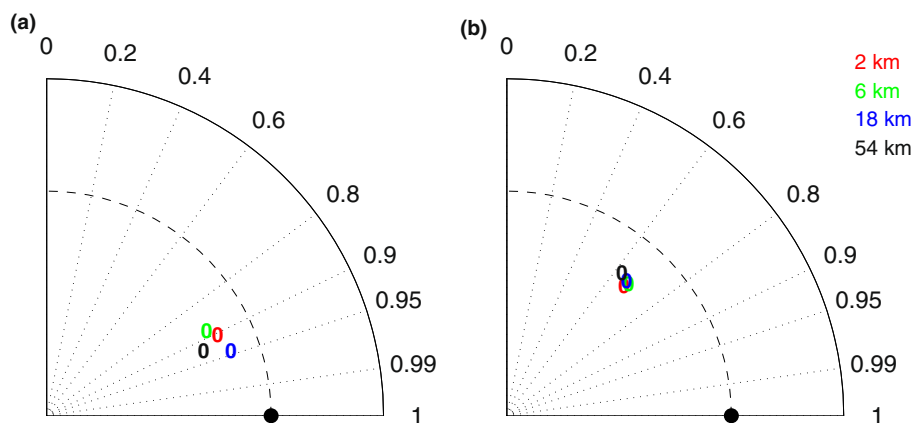
however, small. For the wind speed, all the higher resolution results have a small bias and also seem to have a reasonable diurnal cycle. For the three nested domains the wind speed biases range from −0.1 to 0.6 m s^{−1} and the correlations are ∼0.8 to 0.9. The smallest bias is found in the 2-km results and the largest correlation is found for the 6-km results; for the coarsest resolution results the bias is 2.5 m s^{−1} while the correlation drops to ∼0.5.

Taylor diagrams (Taylor 2001) provide a powerful tool for comparing model results with observations in an objective manner. In this polar-plot technique, the cosine of the angle is proportional to the correlation between the observations and the model (hence zero angle indicates maximum correlation) while the radius indicates the variability. Here, the modelled variability is scaled with the observed variability and hence a perfect model would lie at unity on the x-axis. It can easily be shown that the root-mean-square error (RMSE) is proportional to the distance between this “perfect point” and an actual model point (Taylor 2001). Hence, the same RMSE can be due both to high correlation combined with poor variability and vice versa.

We apply this technique for the different resolutions using all the radio sounding data (e.g. Fig. 7). For the potential temperature (Fig. 13a), we see that the correlation is quite high, but the simulated variability is lower than in the observations for all resolutions. Also, we can see that the differences between the different resolutions do not follow the resolution; the 18- has the lowest RMSE, followed by the 2- and 54-km resolution; the 6-km results have the largest RMSE. For wind speed (Fig. 13b) the correlation between model and observations is lower, which is found in many model evaluations (e.g. Tjernström et al. 2005), and thus the RMSE is larger than for temperature. The differences between the different resolutions are very small, smaller than for temperature, but here the RMSE follows resolution with the 54-km results having the largest objective error and 2-km resolution the smallest; only the lowest resolution results are clearly separated from the rest of the results.

The fact that adding resolution does not seem to provide objective improvement, even when we see additional plausible detail, is problematic but can easily be understood in the following simplified way. Consider the variance of the error in a variable $\sigma_e^2 = \overline{(M - O)^2}/N$, where M is the modelled variable, O is the observation and N is the sample size. This can be expanded as $\sigma_e^2 = (\overline{M^2} + \overline{O^2} - 2\overline{OM})/N$. Since the observations remain the same regardless of model resolution, the change in the error between two model resolutions is $\Delta\sigma_e^2 = (\overline{M_2^2} - \overline{M_1^2} - 2(\overline{OM_2} - \overline{OM_1}))/N$, where index “2” indicates higher resolution than index “1”. Hence, for

Fig. 13 Taylor diagram for **a** potential temperature (K) and **b** wind speed (m s^{-1}) using COAMPS[®] results at 2-, 6-, 18- and 54-km resolutions (see figure legends) and radiosonde observations. See the text for a discussion



model results at different resolution where only the details around a common average differ, the objective error would grow with higher resolution, as $\overline{M_2^2} > \overline{M_1^2}$, and will only decrease if the correlation between modelled and observed values increases more than the variance of the modelled values does. This is a tough criterion to meet especially as the resolution of the observations remains unchanged.

7 Conclusions

We have analysed the importance of spatial resolution in atmospheric modelling of coastal flows, in particular for CLLJs, using the US Navy's COAMPS[®] model. The study is loosely based on a real case, using observations from the US Navy's NPS 2004 summer cruise, on board the R/V Point Sur on a research expedition along the California coast between Pt. Sur and Pt. Conception. While this is not a model evaluation study, a brief assessment of the model results using soundings from this cruise and buoy data, as well as a subjective examination of the features of the coastal jet, provide credibility to the study by illustrating the ability of COAMPS[®] to simulate this type of flow realistically. Our main conclusions are:

1. Adding horizontal resolution provides added realistic detail. However, some model results do not seem to converge for all aspects of the CLLJ, even at the 2-km resolution. In terms of the dimensions of the CLLJ, all three higher resolutions agree reasonably; the CLLJ width at these resolutions also conforms to the Rossby radius of deformation. In terms of the location of the jet, there is reasonable agreement between the two highest resolutions, at 2 and 6 km, while the CLLJ seems to drift farther offshore at the two coarser resolutions; at the coarsest resolution, 54 km, it is also moved south. The extreme maximum wind speed in the jet core continues to increase with resolution all the

way to the 2-km results, while the CLLJ core moves closer to the coast line and is reduced in size. Also the strength of the wind forcing on the coastal ocean seems to grow at increasing resolution.

2. While analysing the results at different resolutions with simple standard objective skill scores, such as bias and RMSE, the results are mixed; the best agreement with the observations are not necessarily always found for the highest resolution domain. Conversely, the larger scale average of the higher resolution results does not agree with coarser scale results, hence there is high-resolution forcing and dynamics which impacts also the larger scale dynamics. Recall that one very effective way to reduce the RMSE in a model is to reduce the variability of the model by, for example, adding numerical diffusion (or reducing the resolution). Hence, adding detail (increasing the variance) in the model affects the objective error adversely unless it is compensated by an increase in the correlation to the observations. We, therefore, need to develop evaluation methods that deal with the temporal and spatial variability in high-resolution modelling in a way that does not penalize higher variability just because there are no observations at that same spatio-temporal resolution.
3. On balance, we conclude that of the resolutions available here, the 6-km resolution is a reasonable compromise to reproduce most of the features of this coastal jet. Moving to coarser resolutions results in a significant loss of mesoscale structure and in reduced wind speeds, along with a significant shift of all features seaward. Increasing resolution to 2 km changes some aspects of the flow, importantly the exact location and strength of the absolute maximum of the wind speed. Hence, increasing resolution from 6 to 2 km adds more detail than it changes structure, while requiring significantly more computer resources; the computational cost may arguably not be motivated

unless particularly sensitive features are of primary interest.

It should be noted that there is nothing specific with the actual resolutions used here; starting with 54 km the rest follows by model default. The conclusion above can be interpreted as the resolution should be less than $O(10\text{ km})$ but can be larger than $O(1\text{ km})$. This analysis could also benefit further from studying more cases or by generating an ensemble of results for this the same case. Also, it should be noted that although the results should be valid for CLLJs worldwide, the results do not necessarily apply for other types of low-level jets, such as nocturnal jets or katabatic flows. In both these cases, the vertical resolutions is likely of larger importance while the horizontal aspects are less critical.

Acknowledgments Semedo acknowledges funding through SHARE (RECI/GEO-MET/0380/2012) and the SOLAR projects (PTDC/GEOMET/7078/2014), Portuguese Foundation for Science and Technology. The authors are grateful to the Naval Research Laboratory's Marine Meteorology Division in Monterey, California, for granting access to the COAMPS[®], and to the colleagues there that develop the model for helping with many practical things. The model simulations were performed on Ekman at PDC, KTH, Sweden.

References

- Beardsley RC, Dorman CE, Friehe CA, Rosenfield LK, Wyant CD (1987) Local atmospheric forcing during the Coastal Ocean Dynamics Experiment 1: a description of the marine boundary layer and atmospheric conditions over a northern California upwelling region. *J Geophys Res* 92:1467–1488
- Bengtsson L, Tijm S, Vanja F, Svensson G (2012) Impact of flow dependent horizontal diffusion on resolved convection in AROME. *J Appl Meteorol* 51:54–67
- Bond NA, Mass CF, Smull BF, Houze RA, Yang M-J, Colle BA, Braun SA, Shapiro MA, Colman BR, Neiman PJ, Overland JE, Neff WD, Doyle JD (1996) The coastal observation and simulation with topography (COAST) experiment. *Bull Am Meteorol Soc* 78:1941–1955
- Bonner WD (1968) Climatology of the low-level jet. *Mon Weather Rev* 96:833–850
- Burk SD, Haack T (2000) The dynamics of wave clouds upwind of coastal orography. *Mon Weather Rev* 128:1438–1455
- Burk SD, Thompson WT (1996) The summertime low-level jet and marine boundary layer structure along the California coast. *Mon Weather Rev* 124:668–686
- Burk SD, Haack T, Samelson RM (1999) Mesoscale simulation of supercritical, subcritical and transcritical flow along coastal topography. *J Atmos Sci* 56:2780–2795
- Burk SD, Haack T, Hodur RM (2001) Orographically forced variability in the coastal marine atmospheric boundary layer. *Fluid Dyn Appl* 61:111–118
- Chen M, Fu C (2000) A nest procedure between regional and global climate model and its application in long term climate simulations (in Chinese). *Chin J Atmos Sci* 24:253–262
- Christensen J, Kuhry HP (2000) High resolution regional climate model validation and permafrost simulation for the East-European Russian Arctic. *J Geophys Res* 105:29647–29658
- Colby FP (2004) Simulation of the New England sea breeze: the effect of grid spacing. *Weather Forecast* 19:277–285
- Cui Z, Tjernström M, Grisogono B (1998) Idealized simulations of atmospheric coastal flow along the central coast of California. *J Appl Meteorol* 37:1332–1363
- Dee DP, Uppala SM, Simmons AJ, Berrisford P, Poli P, Kobayashi S, Andrae U, Balmaseda MA, Balsamo G, Bauer P, Bechtold P, Beljaars ACM, van de Berg L, Bidlot J, Bormann N, Delsol C, Dragani R, Fuentes M, Geer AJ, Haimberger L, Healy S, Hersbach H, Holm EV, Isaksen L, Kållberg P, Kohler M, Matricardi M, McNally AP, Monge-Sanz BM, Morcrette JJ, Peubey C, de Rosnay P, Tavolato C, Thepaut JN, Vitart F (2011) The ERA-Interim reanalysis: configuration and performance of the data assimilation system. *Q J R Meteorol Soc* 136:1972–1990
- Dorman CE, Koračin D (2008) Response of the summer marine layer flow to an extreme California coastal bend. *Mon Weather Rev* 136:2894–2922
- Dorman CE, Rogers DP, Nuss W, Thompson WT (1999) Adjustment of the summer marine boundary layer around Point Sur, California. *Mon Weather Rev* 127:2143–2159
- Douglas MW (1995) The summertime low-level jet over the Gulf of California. *Mon Weather Rev* 123:2334–2347
- Doyle JD, Warner TT (1991) A Carolina coastal low-level jet during GALE IOP 2. *Mon Weather Rev* 119:2414–2428
- Gao X, Shi Y, Song R, Giorgi F, Wang Y, Zhang D (2008) Reduction of future monsoon precipitation over China: comparison between a high resolution RCM simulation and the driving GCM. *Meteorol Atmos Phys* 100:73–86
- Giorgi F, Mearns LO (1991) Approaches to regional climate change simulation: a review. *Rev Geophys* 29:191–216
- Giorgi F, Brodeur CS, Bates GT (1994) Regional climate change scenarios over the United States produced with a nested regional climate model. *J Clim* 7:375–399
- Haack T, Burk SD, Dorman C, Rogers D (2001) Supercritical flow interaction within the Cape Blanco-Cape Mendocino orographic complex. *Mon Weather Rev* 129:688–708
- Haack T, Burk SD, Hodur RM (2005) US West Coast surface heat fluxes, wind stress, and wind stress curl from a mesoscale model. *Mon Weather Rev* 133:3202–3216
- Harshvardhan Davies R, Randall D, Corsetti T (1987) A fast radiation parameterization for atmospheric circulation models. *J Geophys Res* 92:1009–1016
- Hodur RM (1997) The Naval Research Laboratory's coupled ocean/atmosphere mesoscale prediction system (COAMPS). *Mon Weather Rev* 125:1414–1430
- Holt TR (1996) Mesoscale forcing of a boundary layer jet along the California coast. *J Geophys Res* 101:4235–4254
- Hsu H-M, Oey L-Y, Johnson W, Dorman C, Hodur R (2007) Model wind over the central and southern California coastal ocean. *Mon Weather Rev* 135:1931–1944
- Jones RG, Murphy JM, Noguier M (1995) Simulation of climate change over Europe using a nested regional climate model. Part I: assessment of control climate, including sensitivity to location of lateral boundaries. *Q J R Meteorol Soc* 121:1413–1449
- Ju LX, Wang HJ (2006) Modern climate over East Asia simulated by a regional climate model nested in a global grid point general circulation model (in Chinese). *Chin J Geophys* 49:52–60
- Kain JS, Fritsch JM (1990) A one-dimensional entraining/detraining plume model and its application in convective parameterization. *J Atmos Sci* 47:2784–2802
- Leung LR, Wigmosta MS, Ghan SJ, Epstein DJ, Vail LW (1996) Application of a subgrid orographic precipitation/hydrology scheme to a mountain watershed. *J Geophys Res* 101:12803–12817

- Li J, Chen YL (1998) Barrier jets during TAMEX. *Mon Weather Rev* 126:959–971
- Machenhauer B, Windelband M, Botzet M, Christensen JH, Deque M, Jones R, Ruti PM, Visconti G (1998) Validation and analysis of regional present-day climate and climate change simulations over Europe. MPI Report No. 275, MPI, Hamburg, Germany
- Marchesiello P, McWilliams JC, Schepetkin A (2003) Equilibrium structure and dynamics of the California current system. *J Phys Oceanogr* 33:753–783
- Mass CF, Ovens D, Westrick K, Colle BA (2002) Does increasing horizontal resolution produce more skillful forecasts? *Bull Am Meteorol Soc* 83:407–430
- Mellor GL, Yamada T (1982) Development of a closure model of geophysical flows. *Rev Geophys* 20:851–875
- Neiburger M, Johnson DS, Chien C-W (1961) Studies of the structure of the atmosphere over the Eastern Pacific Ocean in summer, vol 1., University of California Publications in meteorology University of California Press, California **58 pp**
- Nicholson SE (2010) A low-level jet along the Benguela coast, an integral part of the Benguela current ecosystem. *Clim Change* 99:613–624
- Nuss WA, Bane JM, Thompson WT, Holt T, Dorman CE, Ralph FM, Rotunno R, Klemp JB, Skamarock WC, Samelson RM, Rogers AM, Reason C, Jackson P (2000) Coastally trapped wind reversals: progress toward understanding. *Bull Am Meteorol Soc* 81:719–743
- Overland JE, Bond NA (1996) Observations and scale analysis of coastal wind jets. *Mon Weather Rev* 123:2934–2941
- Pickett MH, Paduan JD (2003) Ekman transport and pumping in the California current based on the US Navy's high-resolution atmospheric model, COAMPS. *J Geophys Res* 108:3327
- Rahn DA, Parish TR (2007) Diagnosis of the forcing and structure of the coastal jet near Cape Mendocino using in situ observations and numerical simulations. *J Appl Meteorol Climatol* 46:1455–1468
- Rahn DA, Garreaud RD, Rutllant JA (2011) The low-level atmospheric circulation near Tongoy Bay-Point Lengua de Vaca (Chilean Coast, 30°S). *Mon Weather Rev* 139:3628–3647
- Ranjha R, Tjernström M, Semedo A, Svensson G (2015) Structure and variability of the Oman coastal low-level jet. *Tellus* 67:25285. doi:10.3402/tellusa.v67.25285
- Ranjha R, Svensson G, Tjernström M, Semedo A (2013) Global distribution and seasonal variability of coastal low-level jets derived from ERA-Interim reanalysis. *Tellus A*. doi:10.3402/tellusa.v65i0.20412
- Rogers DP, Dorman CE, Edwards KA, Brooks IM, Melville WK, Burk SD, Thompson WT, Holt T, Ström LM, Tjernström M, Grisogono B, Bane JM, Nuss WA, Morley BM, Schanot AJ (1998) Highlights of coastal waves 1996. *Bull Am Meteorol Soc* 79:1307–1326
- Rutledge SA, Hobbs P (1983) The mesoscale and microscale structure and organization of clouds and precipitation in midlatitude cyclones. VIII: a model for the “seeder-feeder” process in warm-frontal rainbands. *J Atmos Sci* 40:1185–1206
- Salathé EP, Steed R, Mass CF, Zahn PH (2008) A high resolution climate model for the US Pacific Northwest: mesoscale feedbacks and local responses to climate change. *J Clim* 21:5708–5726
- Samelson RM (1992) Supercritical marine-layer flow along a smoothly varying coastline. *J Atmos Sci* 49:1571–1584
- Semedo A (2004) Measurements of the California low level coastal jet using radiosondes. Cruise report, Naval Postgraduate School, Monterey, USA. <http://www.weather.nps.navy.mil/~psguest/OC3570/CDROM/summer2004/Semedo/report.pdf>
- Skamarock WC (2004) Evaluating mesoscale NWP models using kinetic energy spectra. *Mon Weather Rev* 132:3019–3032
- Soares PMM, Cardoso R, Semedo A, Chinita M, Ranjha JR (2014) The Iberian Peninsula coastal low level jet. *Tellus A*. doi:10.3402/tellusa.v66.22377
- Steenefeldt GJ, Mauritsen T, De Bruijn EIF, Vilà-Guerau de Arellano J, Svensson G, Holtslag AAM (2008) Evaluation of limited area models for the representation of the diurnal cycle and contrasting nights in CASES99. *J Appl Meteorol Climatol* 47:869–887
- Ström L, Tjernström M (2004) Variability in the summertime coastal marine atmospheric boundary-layer off California, USA. *Q J R Meteorol Soc* 130:423–428. doi:10.1256/qj.03.12
- Ström L, Tjernström M, Rogers DP (2001) Observed dynamics of topographically forced flow at Cape Mendocino during Coastal Waves 1996. *J Atmos Sci* 58:953–977
- Taylor KE (2001) Summarizing multiple aspects of model performance in a single diagram. *J Geophys Res* 106:7183–7192
- Thompson WT, Haack T, Doyle JD, Burk SD (1997) A nonhydrostatic mesoscale simulation of the 10–11 June 1994 coastally trapped wind reversal. *Mon Weather Rev* 125:3211–3230
- Tjernström M (1999) Sensitivity of coastal atmospheric supercritical flow to ambient conditions. *Tellus* 51:880–901
- Tjernström M, Grisogono B (2000) Simulations of supercritical flow around points and capes in the coastal atmosphere. *J Atmos Sci* 57:108–135
- Tjernström M, Žagar M, Svensson G, Cassano JJ, Pfeifer S, Rinke A, Wyser K, Dethloff K, Jones C, Semmler T, Shaw M (2005) Modeling the Arctic boundary layer: an evaluation of six ARCMIP regional-scale models with data from the SHEBA project. *Boundary-Layer Meteorol* 117:337–381
- Toniazzo T, Abel SJ, Wood R, Mechoso CR, Allen G, Shaffrey LC (2011) Large-scale and synoptic meteorology in the south-east Pacific during the observations campaign VOCALS-Rex in austral spring 2008. *Atmos Chem Phys* 11:4977–5009
- Uccellini LW, Johnson DR (1979) The coupling of upper and lower tropospheric jet streams and implications for the development of severe convective storms. *Mon Weather Rev* 107:682–703
- Wetzel MA, Thompson WT, Valli G, Chai SK, Haack T, Szumowski MJ, Kelly R (2001) Evaluation of COAMPS forecasts of coastal stratus using satellite microphysical retrievals and aircraft measurements. *Weather Forecast* 16:588–599
- Winant CD, Dorman CE, Friehe CA, Beardsley RC (1988) The marine layer off northern California: an example of supercritical channel flow. *J Atmos Sci* 45:3588–3605
- Zemba J, Friehe CA (1987) The marine boundary layer jet in the coastal ocean dynamics experiment. *J Geophys Res* 92:1489–1496